ACS Catalysis

Letter

pubs.acs.org/acscatalysis

Highly Active Heterogeneous 3 nm Gold Nanoparticles on Mesoporous Carbon as Catalysts for Low-Temperature Selective Oxidation and Reduction in Water

Shuai Wang,[#,†] Jie Wang,[#,†] Qingfei Zhao,[†] Dandan Li,[†] Jian-Qiang Wang,[‡] Minhyung Cho,[§] Haesung Cho,[§] Osamu Terasaki,[§] Shangjun Chen,[†] and Ying Wan*[,†]

[†]The Education Ministry Key Lab of Resource Chemistry, Shanghai Key Laboratory of Rare Earth Functional Materials, and Department of Chemistry, Shanghai Normal University, Shanghai 200234, P. R. China

[‡]Shanghai Synchrotron Radiation Facility (SSRF), Shanghai Institute of Applied Physics, Chinese Academy of Sciences, Shanghai 201204, P. R. China

[§]Center for Functional Nanomaterials, Department of Chemistry, Korea Advanced Institute of Science and Technology, Daejeon 305-701, Korea

Supporting Information

ABSTRACT: Gold nanoparticles approximately 3 nm in diameter free of protecting agent were loaded onto less-interacting, self-assembling mesoporous carbon using a two-step carbonization method. The catalyst exhibits TOF value of 478 and 31.2 h^{-1} at 25 and 0 °C, comparable to, and much higher than an 8.9 nm gold-supported nanocatalyst, respectively, for the water-mediated selective oxidation of benzyl alcohol. These results highlight the improvement in the sorption of dioxygen species on surface atoms of gold nanoparticles at low temperatures due to electronic modification by the reduction of the particle size.

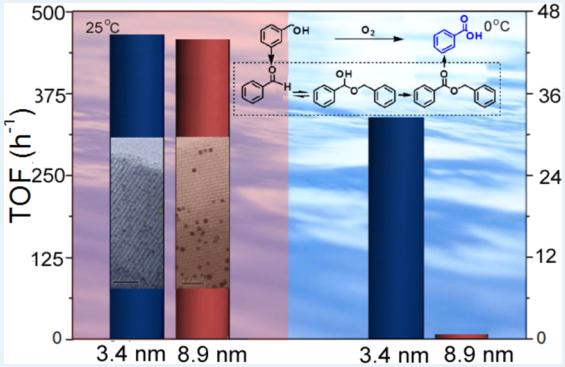

KEYWORDS: *gold nanoparticles, free of protecting agent, low-temperature oxidation, size dependent, mesoporous carbon*

The rapidly increasing interest in gold stems from the fact that the turnover frequency is strongly related to the size of metallic gold particles.[1] For example, optimal oxidation performance is typically achieved when the particle diameter is less than 5 nm.[2] Oxide supports such as TiO_2, CeO_2, and Fe_2O_3 are typically used to isolate small metal nanoparticles with a narrow size distribution.[3] However, the interaction between gold and the support may be critical for the catalytic activity, for example, the stabilization of positive and negative gold atoms at the interphase.[4] To take advantage of the particle size effect while minimizing the interface interaction effect for gold nanoparticles, a less-interacting support such as activated carbon is required.[5]

Current research related to gold on activated carbon severely lags that related to gold on oxides, possibly because of gold's redox properties and the ease of reducing Au(III) precursors, resulting in the formation of large metallic aggregates.[6] A colloidal deposition method was first developed by Prati and Rossi to obtain 3 nm gold particles on activated carbon; the resulting catalyst was highly active toward the liquid-phase oxidation of alcohols by O_2.[7] Protecting groups are always used; they influence the overall activity of gold catalysts in a variety of ways, such as by determining the particle size, the position of the Au NPs on the support surface, and the steric hindrance or electronic modification.[8] Another problem that arises when using supported gold catalysts is that the active sites in postsynthesis catalysts decrease rapidly during heating because gold nanoparticles tend to aggregate at high temperatures. The intercalation of nanoparticles inside carbon frameworks is an attractive solution to this problem. For example, nanocasting methods have been developed, where mesoporous silicates or organosilicates confined with 2−7 nm gold nanoparticles in the walls are used as hard templates.[9] A replication process then yields mesoporous carbon-supported gold.[10] However, the performance of carbon-supported gold catalysts in oxidation reactions is not superior to that of a silica-based analogue because of the growth of nanoparticles from 2 to 7 nm upon high-temperature treatment. Very recently, our group developed a coordination-assisted self-assembly approach to the intercalation of monodispersed gold nanoparticles inside mesoporous carbon walls.[11] A complete conversion of benzyl alcohol in water to benzoic acid can be achieved with this

Received: September 21, 2014
Revised: December 26, 2014
Published: December 28, 2014

DOI: 10.1021/cs501896c
ACS Catal. 2015, 5, 797−802

catalyst at 90 °C and 1 MPa. The limitation of this method, however, is that the particle size is fixed to 9 nm in diameter. The reduction of the gold particle size is urgently needed to investigate its effect on the catalytic performance so that further improvements can be achieved.

The selective oxidation of alcohols is one of the most important transformations in organic synthesis. Recent research interests have been focused on using molecular oxygen at low temperatures (particularly for alcohols with high melting points or low stability at high temperatures), benign solvents, and reusable heterogeneous catalysts, which are favorable from environmental and economic points of view.[12] However, examples of these reactions being performed at room temperature are limited.[13] Herein, we report the first demonstration of the formation of 3.4 nm gold nanoparticles on ordered mesoporous carbon in the absence of a protecting agent. The resulting catalyst exhibits a much higher turnover frequency value in the selective aerobic oxidation of benzyl alcohol at room temperature than has been previously reported, even compared to the reaction run using a 8.9 nm gold-supported nanocatalyst at the freezing point of water. This enhancement in performance is attributed to the coordination effect of small particles.

As previously mentioned, the growth of gold nanoparticles always occurs during high-temperature treatment because of the low melting point of gold nanoparticles and their mobility. Therefore, we reasoned that if the reduction from gold ions to gold and the mobility of gold can be inhibited, particle growth might also be inhibited. Thiol functional groups (here, 3-mercaptopropyl-trimethoxysilane, MPTMS),[14] which are frequently used to protect gold ions, were added into the synthesis batch containing gold ions, low-polymerzied phenolic resins and triblock copolymer. The as-synthesized gold−thiol-silica-resin thin films that were obtained from the solvent evaporation-induced self-assembly of triblock copolymer possessed an S/Au ratio of 32.7. A two-step carbonization that included a treatment with concentrated sulfuric acid and a heating process from room temperature to 600 °C was adopted, and the final product was labeled 3 nm−Au-C. For comparison, 9 nm−Au-C was also synthesized according to the method described in the literature,[11] and we obtained 100 nm Au&C by omitting MPTMS in the synthesis.

The FT-IR spectrum for as-prepared 9 nm−Au-C exhibits several bands corresponding to the characteristic stretching modes of phenolic resins, silicate, and triblock copolymer F127 (Supporting Information (SI) Figure S1), indicative of the formation of an organic−inorganic composite. After treatment with sulfuric acid, the color of the as-prepared 3 nm−Au-C changed from yellow to dark-brown, corresponding to the carbonization of resins. The observed stretching modes associated with the benzene rings changed, and those associated with the surface hydroxyl groups disappeared, further indicating polymerization of the framework. Additionally, the intensities of the C−H vibrations decreased, indicating the partial removal of F127. The nitrogen adsorption−desorption isotherms of the as-prepared 3 nm−Au-C exhibit typical type-IV behavior (SI Figure S2), with a BET surface area of the 3 nm−Au-C of 66 m^2/g, whereas the isotherm of the as-prepared 9 nm−Au-C shows an undetectable surface area. The opened pores in the as-prepared 3 nm−Au-C can be attributed to the carbonization of a triblock copolymer inside the mesopores by concentrated sulfuric acid, in agreement with the IR results. The TG curve for the as-prepared 3 nm−Au-C exhibits two predominant mass losses, which are related to the elimination of the triblock copolymer and resins, respectively, accompanied by the release of small molecules (SI Figure S3). Compared with the triblock copolymer and resin contents of the 9 nm−Au-C, those of the 3 nm−Au-C are much smaller, suggesting a partially carbonized triblock copolymer and resin framework. Concentrated sulfuric acid has also been used as an agent used to carbonize both resins and triblock copolymers.[15]

The C−S stretching mode at 690 cm^{-1} was also clearly observed in the spectra of both the as-prepared 3 nm−Au-C and the 9 nm−Au-C, but not in the spectrum of the sample of thiol-free as-prepared 100 nm Au&C.[16] Evidence for the bonding of the thiol functional groups to composites was also provided by the obtained XPS spectra (SI Figure S4). The binding energy of S $2p_{3/2}$ for the as-prepared 3 nm−Au-C split into two peaks at 163.3 and 164.1 eV, confirming the formation of Au−S and the residue of unreacted −SH. Additionally, the doublet with binding energies of 84.7 and 88.5 eV were similar to those of Au(I) in an alkanethiolate complex for Au $4f_{7/2}$ and $4f_{5/2}$.The wide-angle XRD patterns of as-prepared materials of both 3 nm−Au-C and 9 nm−Au-C show only one diffuse diffraction peak at approximately 23°, providing evidence for the formation of the polymeric-silica compositions (SI Figure S5). Metallic gold was not observed in the XRD images. By comparison, the reduction of metallic gold in as-prepared 100 nm Au&C occurred, demonstrating the essential role of coordination between Au and −SH for the stabilization of Au ions.

Upon carbonization at 600 °C and the elimination of silica, carbon-supported gold catalysts were obtained. EDX analysis revealed the presence of Au, C, and O (SI Figure S6A). No sulfur residue was detected, suggesting that the functional groups were volatilized during calcinations, similar to gold-containing mesoporous silicates.[9c−e] The XPS spectrum displays indistinct binding energy for S 1s, further elucidating the presence of S in the catalyst (SI Figure S6B). The gold content for the studied catalysts is approximately 5.3 wt %, as determined by ICP-AES (SI Table S1). The XRD patterns for 3 nm−Au-C show relatively diffuse diffractions in a wide-angle range belonging to fcc Au, and typical diffractions corresponding to an ordered mesophase in the small-angle range (Figure 1A,B). The XRD results are similar to those previously reported for 9 nm−Au-C.[11] However, the size of the metallic gold nanoparticles prepared using our method was significantly reduced, as estimated from the rather wide diffraction peak. In contrast, particles larger than 50 nm were clearly detected for 100 nm Au&C, although the ordered mesopore arrays were maintained.[11] N_2 adsorption−desorption isotherms for the 3 nm−Au-C exhibit type-IV curves, indicating a uniform mesopore distribution of approximately 3.4 nm (SI Figure S7, Table S1). The distinct increase in sorption shown in the isotherm curves at low relative pressures of P/P_0 of 0.01−0.3 implies the presence of a large amount of small pores approximately 2 nm in size.[17] High surface areas of 1269 m^2/g and large pore volumes of 0.79 cm^3/g were achieved because of a large number of voids.

The FT-EXAFS spectra of the immobilized Au particles show features analogous with those of gold foil, indicative of the metallic state of the carbon-supported gold catalysts (Figure 1C). The Au−Au contribution, distance, and coordination number decreases with decreasing particle size (SI Table S2). The intensities of the metallic peak at ∼ 11.92 keV in the XANES features decrease in the order of 100 nm Au&C

DOI: 10.1021/cs501896c
ACS Catal. 2015, 5, 797−802

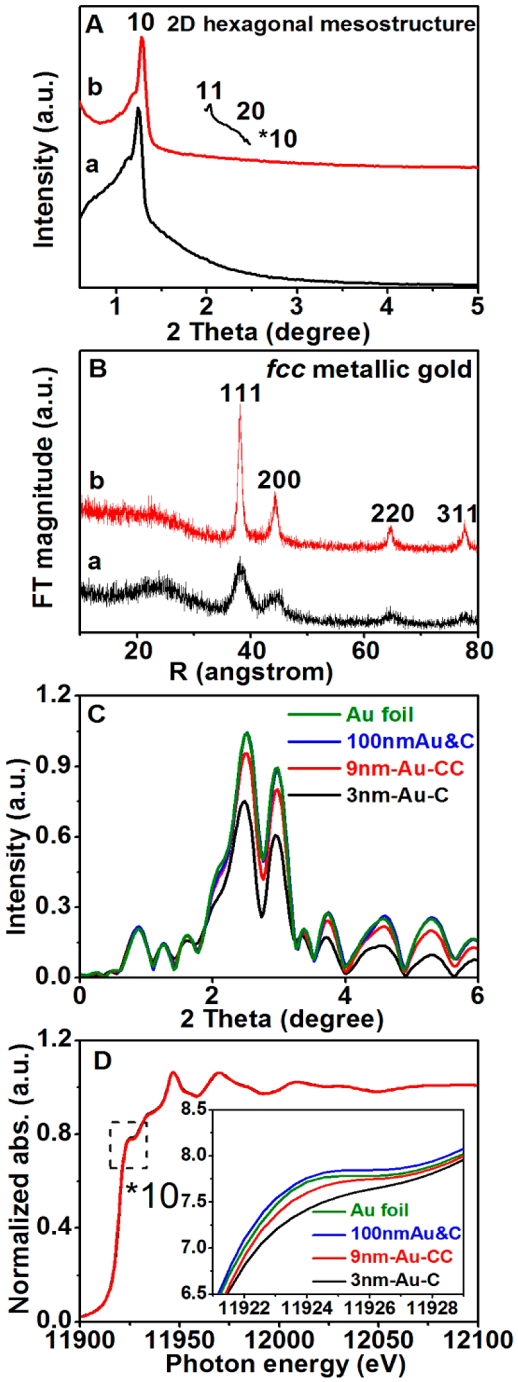

Figure 1. (A) Small-angle and (B) wide-angle XRD patterns, and (C) FT-EXAFS and (D) XANES spectra for (a) 3.4 and (b) 8.9 nm gold particles on carbon.

(similar to Au foil) > 9 nm−Au-C > 3 nm−Au-C, indicating a change in the electronic properties of gold nanoparticles (Figure 1D). Given that the carbon support is less-interacting, this fact is possibly related to the size of the gold nanoparticles. The smaller particles in 3 nm−Au-C have a shorter Au−Au distance, which favors enhanced *d*-*d* interactions, narrows the *d*-band, and lowers the energy of the *d*-orbitals.[18]

HRSEM images for the 3 nm−Au-C show a typical rough surface with opened mesopores (Figure 2A). Brighter- and darker-contrast Au nanoparticles with a size of approximately 3.4 nm were observed only after the cross sections were

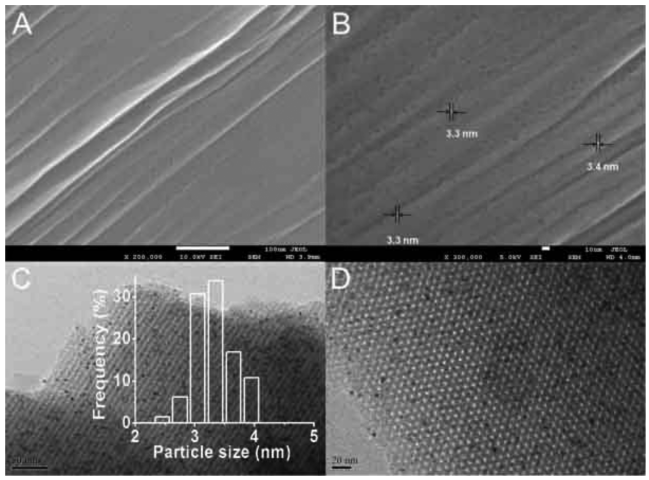

Figure 2. (A,B) HRSEM and (C,D) TEM images of the 3 nm−Au-C: (A) surface, (B) after cross-section polishing, (C) viewed along the (110), and (D) the (001) directions. The particle sizes are labeled with a solid line in (B). The inset in (C) is the metal-particle size distribution histogram.

polished (Figure 2B). These brighter- and darker-contrast Au nanoparticles correspond to particles that are exposed to the surface and covered by carbon thin layers, respectively. These phenomena confirm that the Au nanoparticles were located inside the nanopores rather than on the external surface of the mesostructured solids. TEM images show monodispersed dark gold nanoparticles within the whole catalyst particles and typical stripe-like and hexagonally arranged pores of the 2D hexagonal mesostructure. The nanoparticles have an average size of 3.4 nm (statistically the same as the other samples) with a semiexposure morphology (Figure 2C, D). One portion of the particle is partially exposed to pore channels, and the other is tightly intercalated into the carbon framework. Notably, no large particles outside the ordered mesopores were observed, clearly indicating that the thermally stable gold nanoparticles are confined in the carbonaceous matrix. The nanoparticles of 9 nm−Au-C are approximately 8.9 nm in diameter, and the corresponding images show that these particles occupy both pore channels and adjacent pore walls, but do not penetrate walls.[11]

The formation of small gold nanoparticles is highly related to the S−Au coordination and carbonization procedure.[9,11] In this process, the reduction of gold ions to metallic gold is first inhibited by the strong coordination with the thiol group in the as-synthesized samples. Gold nanoparticles are then reduced and grown at elevated temperatures, accompanied by the release of thiol and other small molecules, which is an exothermic process. The simultaneous formation of gold nanoparticles and relatively rigid silica−carbon framework favors the intercalation of Au in pore walls.[9d,e] But the particle growth is confined by the rigid silica−carbon pore walls with adjacent to six cylindrical pores. The growth is ended with the particle size about 8.9 nm upon carbonization at 600 °C.[11] Unobvious distortion of ordered porosity occurs after gold deposition, although the gold diameter is apparently larger than either pore size or wall thickness. Interestingly, similar nanoparticle sizes were further observed in the catalysts upon being heated from 350 to 900 °C for the same catalyst, although the mesostructured framework significantly shrank (SI Figure S8). This phenomenon differs from that observed in the

DOI: 10.1021/cs501896c
ACS Catal. 2015, 5, 797−802

case of the supported gold catalysts, whose size is temperature dependent, and therefore implies the confinement of the nanoparticles by relatively "rigid" carbonaceous framework even at a relatively low temperature in the present catalyst. In this case, a delayed high-temperature carbonization was adopted. A sulfuric acid treatment step was carried out before calcination to rigidify the carbonaceous pore wall and partially carbonize triblock copolymer. The condensed framework may favor the fixing of gold nanoparticles after they have been reduced. In addition, the less heat liberated by the previously removed CH_4, CO, among others, from F127 and resins also favor the stabilization of gold particles because heat is the main driving force for the mobility of nanoparticles. As a result, the 3 nm gold particles are immobilized.

The selective oxidation of benzyl alcohol with molecular O_2 in water in the presence of base was used to evaluate the activity of the catalysts under mild conditions of 60 °C and atmospheric pressure (Figure 3). The reaction pathway of 3

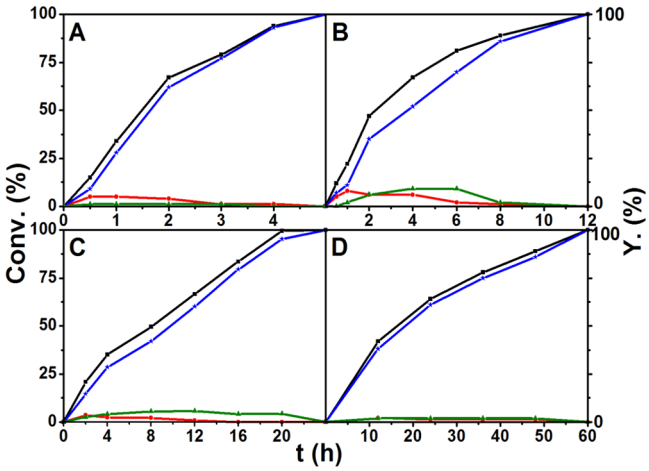

Figure 3. Time-course plots for the conversion of benzyl alcohol (-■-, black) and the yields of benzoic acid (-★-, blue), benzaldehyde (-●-, red), and benzyl benzoate (-▲-, green) over (A,C,D) 3 nm−Au-C, and (B) 9 nm−Au-C at (A,B) 60 °C, (C) 25 °C and (D) 0 °C in water. The Au:substrate was about 1:1800, 1:1600, and 1:360 for (A,C), B and D, respectively. Reaction conditions: 4.8 mmol benzyl alcohol; 14.4 mmol KOH; 10 mL H_2O; 1 atmO_2; 800 rpm.

nm−Au-C, which goes through the intermediates benzaldehyde and benzyl benzoate, is similar to that of 9 nm−Au-C. But the selectivity for benzyl benzoate decreases using 3 nm−Au-C compared to 9 nm−Au-C at the similar benzyl alcohol conversion, implying the improvement of further oxidation of benzaldehyde and the suppression of dehydroesterification reaction between benzaldehyde and benzyl alcohol on the Au surface. The suppression of this byproduct may be ascribed to small areas of the active sites which are intercalated into and isolated by carbon.[19]

A near 100% yield for benzoic acid can be achieved within 5 h using 3 nm−Au-C and within 12 h using 9 nm−Au-C, and the initial reaction rate follows the order 3 nm−Au-C > 9 nm−Au-C. In the case of supported particles, the molar fraction of surface atoms available for catalysis was calculated in each case for gold polyhedra lying on an inactive support, such as graphite or carbon, with a (111)-type face.[20] The TOF values for the Au−C catalysts with sizes of 3.4 and 8.9 nm were then calculated to be 1638 and 2506 h^{-1}, respectively. A decrease in reaction temperature leads to similar TOF values for these two catalysts (478 and 470 h^{-1}). When the reaction system was cooled even further to the freezing point of water, the 3 nm−Au-C exhibited a much higher activity in the conversion of benzyl alcohol with a TOF value of 31.2 h^{-1}, whereas the 9 nm−Au-C exhibited an extremely low conversion of benzyl alcohol (<2%) at 0 °C within 60 h. The TOF values for 3 nm−Au-C at low temperatures were also higher than those calculated from the literature values (SI Table S3). Notably, the reaction intermediates are similar, irrespective of the reaction temperature. A similarly inverse TOF value order was found over Au/CeO2 with respect to palladium supported on hydroxyapatite in selective oxidation of benzyl alcohols when the temperature decreases from 160 to 120 °C.[21] Therefore, the comparably high relevance of TOF to temperature of 9 nm−Au-C may also reflect the higher apparent activation energy for alcohol oxidation using 9 nm particles as compared to those of 3 nm gold in the studied temperature range.

The external mass transfer limitations were avoided by stirring at 800 rpm. The Madon−Boudart (MB) test was used to verify the absence of mass transfer effects during the selective oxidation of benzyl alcohol.[22] The MB test requires measurement of the reaction rate (on per mmol metal basis) for catalysts with varying surface concentrations of metal but with similar dispersion. Because the 9 nm−Au-C catalyst possesses the similar pore size with 3 nm−Au-C, but a relative larger gold particle size, the mass transfer effect, if any, should be more serious. We further synthesized two additional samples with different gold contents (1.1, and 2.9 wt %). Monodispersed Au nanoparticles with ∼9 nm in size, ordered mesostructure, high surface areas, large pore volumes and uniform pore sizes can be maintained within the studied Au content, as evidenced by the XRD patterns, N2 sorption isotherms, and TEM images (SI Figure S9, S10, and Table S1). A plot of rate versus surface concentration at 60 °C yields a straight line, demonstrating the mass transfer effect is absent (SI Figure S11). The easy accessibility of gold nanoparticles is related to the abundant secondary voids inside the carbon pore walls. These voids have been reported to facilitate the mass transport of large dye molecules.[23]

Solid catalysts were filtered out of the reaction, and the filtrate was monitored for continued activity.[24] When 3 nm−Au-C is hot filtered, after approximately 34% conversion, the filtrate loses its activity, which is a proof of a negligible gold leaching and heterogeneous catalysis (SI Figure S12). A thiol-functionalized mesoporous silica (SH-SBA-15) solid was also introduced into the reaction batch after the addition of the supported 3.4 nm gold catalyst at 60 °C and at an S/Au ratio of approximately 35 to trap leached gold ions.[25] The indistinct change in the conversion plots in the presence of the thiol groups excludes the activity associated with leached gold and provides further evidence for the surface-driven catalysis.

These results indicate that selective oxidation of benzyl alcohol undergoes a size-dependent catalysis over ligand-less gold nanoparticles, especially at lower temperatures. The Au−C-catalyzed reaction may involve the adsorption of a superoxo-like molecular oxygen species on the Au nanoparticles.[20,26] The coordination effect on the Fermi energy levels of the 3.4 nm gold nanoparticles and the subsequent variation of the *d*-band contribution to the total chemisorption energy of the gold particles,[27] as evidenced by the XAFS results, is reasonably explained in terms of the efficient activation of O2 by small-sized gold nanocatalysts at low temperatures. It should be mentioned that the size-dependent catalysis was established

DOI: 10.1021/cs501896c
ACS Catal. 2015, 5, 797−802

with the particle sizes of 3.4 and 8.9 nm. A metal-to-nonmetal transition for gold below 2 nm is not involved.[28]

The reduction of *p*-nitrophenol by sodium borohydride over the 3.4 nm gold nanocatalyst at 0 °C in water was also investigated. A complete yield of *p*-aminophenol was achieved in 10 min with a TOF value of 1.70 min^{-1}. The trapping agent of SH-SBA-15 for leached gold exhibits a negligible effect on the conversion plots. Infiltration of the solid catalyst after 3 min can completely quench the activity, further demonstrating the negligible gold leaching and heterogeneous surface-driven catalysis. The conversion of *p*-nitrophenol remained nearly the same during the first 2 min over the reused catalyst for 5 cycles (SI Figure S13), demonstrating its reusability. The aqueous solution was collected after each cycle and contained undetectable amounts of gold. The catalyst, after three cycles, was characterized. Negligible leaching gold was detected for the solid catalyst by ICP-AES (Table S1). The TEM image shows the stripe-like and hexagonally arranged pore arrays of the catalyst, containing highly dispersed nanoparticles with a size of about 3.4 nm, demonstrating that the heterogeneous catalyst is stable, and the reaction conditions have minor effects on the catalyst structure (SI Figure S14). The XRD pattern and N2 sorption isotherms further confirm the stability of the catalyst (SI Figure S15, Table S1). The used catalyst exhibits similar structural and textual properties to the fresh one, indicating that the ordered 2-D hexagonal mesostructure, high surface area, and uniform mesopores of the catalyst are all retained.

In summary, monodispersed gold nanoparticles with a size of ~3 nm were immobilized on ordered mesoporous carbon in the absence of any protecting agent. This catalyst exhibits a high activity toward the selective oxidation of benzyl alcohol to benzyl acid and toward the reduction of *p*-nitrophenol to *p*-aminophenol at low temperatures such as 0 °C. A size-dependent selective oxidation over gold nanoparticles by the exposed surface atoms was observed at 0 °C, whereas the intrinsic activity at 25 °C was independent of size. The electronic modification of the *d*-orbitals of small particles is extremely important for chemisorption at low temperatures.

■ ASSOCIATED CONTENT

Supporting Information

The following file is available free of charge on the ACS Publications website at DOI: 10.1021/cs501896c.

Experimental procedures and characterization data (PDF)

■ AUTHOR INFORMATION

Corresponding Author

*E-mail: ywan@shnu.edu.cn.

Author Contributions

#S.W. and J.W. contributed equally to this work.

Notes

The authors declare no competing financial interest.

■ ACKNOWLEDGMENTS

This work was supported by the State Key Basic Research Program of China (2013CB934102), NSF of China (21322308 and 21173149), Ministry of Education of China (PCSIRT-IRT1269 and 20123127110004), and Shanghai Science and Technology and Education Committee (11JC1409200, DZL123 and S30406).

■ REFERENCES

(1) (a) Corma, A.; Garcia, H. *Chem. Soc. Rev.* **2008**, *37*, 2096−2126. (b) Yamazoe, S.; Koyasu, K.; Tsukuda, T. *Acc. Chem. Res.* **2013**, *47*, 816−824. (c) Li, G.; Jiang, D.; Liu, C.; Yu, C.; Jin, R. *J. Catal.* **2013**, *306*, 177−183.

(2) (a) Ishida, T.; Kinoshita, N.; Okatsu, H.; Akita, T.; Takei, T.; Haruta, M. *Angew. Chem., Int. Ed.* **2008**, *120*, 9405−9408. (b) Ishida, T.; Watanabe, H.; Bebeko, T.; Akita, T.; Haruta, M. *Appl. Catal., A* **2010**, *377*, 42−46.

(3) (a) Li, L.; Gao, Y.; Li, H.; Zhao, Y.; Pei, Y.; Chen, Z.; Zeng, X. C. *J. Am. Chem. Soc.* **2013**, *135*, 19336−19346. (b) Wu, Z.; Jiang, D.-e.; Mann, A. K. P.; Mullins, D. R.; Qiao, Z.-A.; Allard, L. F.; Zeng, C.; Jin, R.; Overbury, S. H. *J. Am. Chem. Soc.* **2014**, *136*, 6111−6122.

(4) (a) Abad, A.; Concepción, P.; Corma, A.; García, H. *Angew. Chem., Int. Ed.* **2005**, *44*, 4066−4069. (b) Wang, Z.-W.; Wang, X. V.; Zeng, D. Y.; Chen, M.-S.; Wan, H.-L. *Catal. Today* **2011**, *160*, 144−152.

(5) Turner, M.; Golovko, V. B.; Vaughan, O. P. H.; Abdulkin, P.; Berenguer-Murcia, A.; Tikhov, M. S.; Johnson, B. F. G.; Lambert, R. M. *Nature* **2008**, *454*, 981−983.

(6) (a) Goguet, A.; Hardacre, C.; Harvey, I.; Narasimharao, K.; Saih, Y.; Sa, J. *J. Am. Chem. Soc.* **2009**, *131*, 6973−6975. (b) Prati, L.; Villa, A.; Lupini, A. R.; Veith, G. M. *Phys. Chem. Chem. Phys.* **2012**, *14*, 2969−2978.

(7) (a) Prati, L.; Rossi, M. *J. Catal.* **1998**, *176*, 552−560. (b) Comotti, M.; Della Pina, C.; Matarrese, R.; Rossi, M. *Angew. Chem., Int. Ed.* **2004**, *43*, 5812−5815. (c) Ma, C.; Xue, W.; Li, J.; Xing, W.; Hao, Z. *Green Chem.* **2013**, *15*, 1035−1041.

(8) (a) Toebes, M. L.; Zhang, Y.; Hájek, J.; Alexander Nijhuis, T.; Bitter, J. H.; Jos van Dillen, A.; Murzin, D. Y.; Koningsberger, D. C.; de Jong, K. P. *J. Catal.* **2004**, *226*, 215−225. (b) Villa, A.; Wang, D.; Su, D.; Veith, G. M.; Prati, L. *Phys. Chem. Chem. Phys.* **2010**, *12*, 2183−2189. (c) Zhong, R.-Y.; Yan, X.-H.; Gao, Z.-K.; Zhang, R.-J.; Xu, B.-Q. *Catal. Sci. Technol.* **2013**, *3*, 3013−3019.

(9) (a) Chen, L.; Hu, J.; Richards, R. *J. Am. Chem. Soc.* **2009**, *131*, 914−915. (b) Besson, E.; Mehdi, A.; Reye, C.; Corriu, R. J. P. *J. Mater. Chem.* **2009**, *19*, 4746−4752. (c) Wu, P.; Bai, P.; Lei, Z.; Loh, K. P.; Zhao, X. S. *Microporous Mesoporous Mater.* **2011**, *141*, 222−230. (d) Zhu, H.; Lee, B.; Dai, S.; Overbury, S. H. *Langmuir* **2003**, *19*, 3974−3980. (e) Lee, B.; Zhu, H.; Zhang, Z.; Overbury, S. H.; Dai, S. *Microporous Mesoporous Mater.* **2004**, *70*, 71−80.

(10) Kerdi, F.; Caps, V.; Tuel, A. *Microporous Mesoporous Mater.* **2011**, *140*, 89−96.

(11) Wang, S.; Zhao, Q.; Wei, H.; Wang, J.-Q.; Cho, M.; Cho, H. S.; Terasaki, O.; Wan, Y. *J. Am. Chem. Soc.* **2013**, *135*, 11849−11860.

(12) Dimitratos, N.; Lopez-Sanchez, J. A.; Hutchings, G. *J. Chem. Sci.* **2012**, *3*, 20−44.

(13) (a) Miyamura, H.; Matsubara, R.; Miyazaki, Y.; Kobayashi, S. *Angew. Chem., Int. Ed.* **2007**, *46*, 4151−4154. (b) Han, J.; Liu, Y.; Guo, R. *J. Am. Chem. Soc.* **2009**, *131*, 2060−2061.

(14) Hakkinen, H. *Nat. Chem.* **2012**, *4*, 443−455.

(15) Zhuang, X.; Zhao, Q.; Wan, Y. *J. Mater. Chem.* **2010**, *20*, 4715−4724.

(16) Ungureanu, S.; Birot, M.; Laurent, G.; Deleuze, H.; Babot, O.; Julián-López, B.; Achard, M.-F.; Popa, M. I.; Sanchez, C.; Backov, R. *Chem. Mater.* **2007**, *19*, 5786−5796.

(17) Liu, R.; Shi, Y.; Wan, Y.; Meng, Y.; Zhang, F.; Gu, D.; Chen, Z.; Tu, B.; Zhao, D. *J. Am. Chem. Soc.* **2006**, *128*, 11652−11662.

(18) Miller, J. T.; Kropf, A. J.; Zha, Y.; Regalbuto, J. R.; Delannoy, L.; Louis, C.; Bus, E.; van Bokhoven, J. A. *J. Catal.* **2006**, *240*, 222−234.

(19) (a) Chen, K.; Wu, H.; Hua, Q.; Chang, S.; Huang, W. *Phys. Chem. Chem. Phys.* **2013**, *15*, 2273−2277. (b) Yoskamtorn, T.; Yamazoe, S.; Takahata, R.; Nishigaki, J.-i.; Thivasasith, A.; Limtrakul, J.; Tsukuda, T. *ACS Catal.* **2014**, *4*, 3696−3700.

(20) Della Pina, C.; Falletta, E.; Rossi, M.; Sacco, A. *J. Catal.* **2009**, *263*, 92−97.

(21) Abad, A.; Almela, C.; Corma, A.; García, H. *Tetrahedron* **2006**, *62*, 6666−6672.

DOI: 10.1021/cs501896c
ACS Catal. 2015, 5, 797−802

(22) (a) Madon, R. J.; Boudart, M. *Ind. Eng. Chem. Fundam.* **1982**, *21*, 438−447. (b) Semagina, N.; Joannet, E.; Parra, S.; Sulman, E.; Renken, A.; Kiwi-Minsker, L. *Appl. Catal., A* **2005**, *280*, 141−147. (c) Rioux, R. M.; Song, H.; Hoefelmeyer, J. D.; Yang, P.; Somorjai, G. A. *J. Phys. Chem. B* **2004**, *109*, 2192−2202. (d) Sun, K.-Q.; Hong, Y.-C.; Zhang, G.-R.; Xu, B.-Q. *ACS Catal.* **2011**, *1*, 1336−1346.
(23) Zhuang, X.; Wan, Y.; Feng, C.; Shen, Y.; Zhao, D. *Chem. Mater.* **2009**, *21*, 706−716.
(24) Sheldon, R. A.; Wallau, M.; Arends, I. W.; Schuchardt, U. *Acc. Chem. Res.* **1998**, *31*, 485−493.
(25) Richardson, J. M.; Jones, C. W. *J. Catal.* **2007**, *251*, 80−93.
(26) (a) Tsunoyama, H.; Sakurai, H.; Negishi, Y.; Tsukuda, T. *J. Am. Chem. Soc.* **2005**, *127*, 9374−9375. (b) Pal, R.; Wang, L.-M.; Pei, Y.; Wang, L.-S.; Zeng, X. C. *J. Am. Chem. Soc.* **2012**, *134*, 9438−9445. (c) Zhang, Y.; Cui, X.; Shi, F.; Deng, Y. *Chem. Rev.* **2011**, *112*, 2467−2505. (d) Tsunoyama, H.; Ichikuni, N.; Sakurai, H.; Tsukuda, T. *J. Am. Chem. Soc.* **2009**, *131*, 7086−7093.
(27) Phala, N.; van Steen, E. *Gold Bull.* **2007**, *40*, 150−153.
(28) (a) Valden, M.; Lai, X.; Goodman, D. W. *Science* **1998**, *281*, 1647−1650. (b) Bond, G. C. *Faraday Discuss.* **2011**, *152*, 277−291.

DOI: 10.1021/cs501896c
ACS Catal. 2015, 5, 797−802